Modeling a broadband terahertz system based on an electro-optic polymer emitter–sensor pair

Xuemei Zheng, Colin V. McLaughlin, Megan R. Leahy-Hoppa, Alexander M. Sinyukov, and L. Michael Hayden

Department of Physics, University of Maryland, Baltimore County, Baltimore, Maryland 21250

We present a model for a broadband terahertz (THz) system that employs electro-optic (EO) polymer films for THz generation via optical rectification and THz detection using EO sampling. In this model, we take the laser spectral bandwidth, pulse distortion, and the material properties of the EO medium into consideration, at both the generation and detection sites, and investigate the roles they play in affecting the performance of the THz system. This model provides us with a guide to select suitable EO materials and proper light sources for bright, broadband THz systems. © 2006 Optical Society of America

OCIS codes: 190.7110, 250.2080, 320.2250.

1. INTRODUCTION

The accessibility of ultrashort terahertz (THz) transient waves and their associated broadband spectra from table-top THz systems based on ultrashort lasers has led to powerful techniques such as THz time-domain spectroscopy (TDS)[1] and THz imaging[2] for the characterization of condensed matter,[3] molecular materials,[4] and biological tissues.[5] To fully utilize the capabilities of THz TDS to obtain linear spectroscopic characteristics across a wide THz spectral range, a detailed understanding of broadband THz emission and detection processes is required. For time-of-flight imaging or tomography based on THz pulses, a high depth resolution requires a shorter pulse width, which in turn also requires a broadband THz spectrum. Thus far, between the two types of broadband table-top THz systems, the optical THz systems[6,7] associated with electro-optic (EO) crystals have demonstrated the advantage of broader bandwidth over the optoelectronic THz systems[8] associated with photoconductive antennas, thanks to wide material selection possibilities and relatively easy material processing for the former. Using a 20 μm z-cut GaSe emitter, a 30 μm z-cut GaSe sensor, and laser pulses with a duration of 10 fs full width at half-maximum (FWHM) and a 103 nm bandwidth centered at 780 nm, Kubler *et al.* have achieved >100 THz bandwidth,[9] although the THz components lower than ~7 THz were missing from their spectrum (possibly due to the phonon absorption of GaSe). At present, phonon absorption associated with the lattice resonance of virtually all inorganic (EO or photoconductive) materials used for THz emitters and sensors is the main reason that the useful range of most THz TDS systems are limited to only 3–5 THz. Yet it is important to extend the continuous spectral coverage range of THz TDS systems to ~10 THz, as the counterpart of THz TDS—Fourier-transform infrared spectrometers—performs poorly in this range.

Because of their high EO coefficients, EO polymers have been demonstrated to be alternatives to inorganic crystals as efficient THz emitters.[10–13] In addition, because of their instantaneous (electronic) response associated with the extended π conjugation and the relatively small dispersion, EO polymers have also been proposed[12] and demonstrated[14] as better sensor materials for broadband THz detection via EO sampling. Recently, we have successfully employed a pair of LAPC [an EO polymer consisting of a guest-host mixture of 40% (3-(2-(4-(N,N-diethylamino)-phenyl)ethenyl)-5,5-dimethyl-1,2-cyclohexenylidene)-propanedinitrile (Lemke) and 60% amorphous polycarbonate] films to achieve a gap-free, ~12 THz response.[15] Such broad and continuous spectral coverage cannot be achieved from conventional inorganic EO materials and accents the advantage of using EO polymers as THz emitters and sensors. The preparation of LAPC has been described elsewhere.[11,12] EO coefficients r_{33} (the element with the highest value in the polymer's EO coefficient matrix) between 25 and 40 pm/V were routinely achieved at 800 nm, in comparison with ~4 pm/V for ZnTe (the most common EO material for THz emission and detection). Because of the present vertical poling configuration, a Brewster-angle incidence for the pump beam is required to achieve the maximum THz emission when using a LAPC emitter.[12] In this situation, the effective nonlinear coefficient is approximately half of χ_{33} ($\chi_{33} = -n^4 r_{33}/4$), which is still much higher than ZnTe. With our polymer emitter–sensor pair, the difference signal from the detection photodiodes, defined as $\Delta I = (I_1 - I_2)/(I_1 + I_2)$, was found to have a maximum value of ~2.5×10^{-3}, where I_1 and I_2 are the photocurrent in two diodes of the differential detection system. Considering the fact that an amplified laser system was used in our experiments, this difference signal is not extremely large. This is explained by the polymer orientation issues at the detection site. When the EO polymer film is used as the THz sensor in EO sampling, the vertical poling configuration keeps us from using normal incidence for the THz and probe beam.[15] For this reason, the EO polymer sensor sees only the projected component (not the full strength) of the incident THz field. Also, this sensor orientation arrangement[16] does not present the best figure of merit (FOM) for EO detection. In contrast, for (110)-cut ZnTe

sensors, it is easy to experimentally achieve the optimal crystal orientation suggested by theory.[17] Taking these factors and the materials' different EO coefficients into consideration, we find that the sensitivity of the LAPC detector is ~1 order of magnitude smaller than (110)-cut ZnTe (not considering the effect of phase mismatching). However, this issue can be solved by resorting to an in-plane poling geometry. Fortunately, there are many novel EO polymers[18,19] possessing much higher EO coefficients than LAPC. Recently, an EO polymer was reported with an $r_{33} > 300$ pm/V at 1310 nm.[20,21] With many EO polymers currently available and many more potentially available, it is crucial at this point to develop a model to guide our material selection for THz emitters and sensors to construct THz systems possessing the required bandwidth and brightness for customized THz applications.

Time-domain[22] and frequency-domain[23] modeling of EO detection of transient THz waves has been performed. Modeling work on the THz generation via optical rectification (OR) has also been done to some degree. Xu and co-workers[24] have obtained an analytical solution for OR in the time domain, neglecting the material dispersion and absorption in both THz and optical regimes (yet these factors are essential to accurately model a broadband THz system). Faure *et al.* derived an analytical solution from a simplified equation for OR in the frequency domain.[25] They, like Xu and co-workers, assumed that the pump pulse was transform limited and that the EO material exhibited no dispersion or absorption in the THz region and no group-velocity dispersion (GVD) in the optical region. These assumptions are not generally valid, especially when the EO medium has a lattice resonance in the THz emission range and when the pump pulses are much shorter than 100 fs. We note that from a practical standpoint, it is difficult to achieve ideal pulse compression where spectrally broad pulses are involved. With the trend of using extremely short pulses to generate and detect ultra-wide-bandwidth THz waves, the effects of using non-transform-limited pulses with a broad spectral bandwidth should also be taken into account. Also, when using sub-50-fs pump pulses, it is possible that the generated THz bandwidth is broad enough to cover the resonance region of a crystalline EO material used as a THz emitter and/or sensor.[15] In this case, the corresponding dispersion and absorption of the material in the THz region cannot be ignored for accurate modeling. Finally, for sub-50-fs pulses associated with a broad spectral bandwidth, the optical GVD of EO materials gives rise to fast pulse broadening, making it necessary to include this issue in the model. Once all of these factors are taken into consideration, an analytical solution for OR no longer exists, making it necessary to use a numerical method to find a solution.

In Section 2, we discuss the origin of pulse distortion of a chirped pulse amplification (CPA) system to obtain an expression for the laser field approximately representing our real experimental conditions. On the basis of this expression of the laser field, we then derive a general propagating nonlinear polarization in an EO material and numerically solve the nonlinear wave-mixing equation for OR in an EO polymer (THz emitter) with this nonlinear polarization as the driving source. For the THz detection site, we modify a model presented by Gallot and Grischkowsky[23] by removing the assumption of transform-limited laser pulses and using the expression of the laser field derived in Section 2 as a more realistic probe pulse. The completed model, presented in Section 3, combines THz generation and detection. In Section 4, we compare the simulation results with experimental results for LAPC emitters with different thicknesses to examine the accuracy of our model. In Section 5 we present our conclusions.

2. PULSE DISTORTION IN A CHIRPED PULSE AMPLIFICATION SYSTEM

Since ultrashort laser pulses play an important role in table-top broadband THz systems, it is essential that we understand the mechanisms that cause pulse distortion during compression and propagation before we can write down a suitable mathematical expression for the laser field. The generation of ultrashort laser pulses always involves some scheme of pulse compression. A CPA system, which is what we use in our experiments, employs a complicated method. Before a seed pulse is injected into the amplifier, its duration is widened in time by going through a carefully designed stretcher that introduces a near-linear frequency chirp, so as to avoid damage to the optics and nonlinear distortion to the pulse when it is amplified. The pulse then makes tens of round trips in the amplifier with the pulse energy amplified by 5–6 orders of magnitude. During this time the pulse experiences additional distortion due to the dispersion of the materials in its optical pathway, including the amplifying medium and EO crystals in the amplifier laser cavity. In the final phase, the sufficiently amplified pulse has to go through a compressor whose linear chirp has the opposite sign with regard to the stretcher, such that it is recompressed toward the duration of the incident seed pulse.

In the ultrashort laser community, the action of an entire amplifier system is often described in the frequency domain. The complex transfer function of the CPA system is expressed by $s(\omega)\exp[i\phi(\omega)]$, where $s(\omega)$ describes the frequency-dependent gain of the amplifier and $\phi(\omega)$ is the spectral phase with contributions from the stretcher, compressor, and materials of the amplifier.[26] For an amplifier system with an ideal compressor in the final phase, all of the frequency components of the output pulse should be in phase at the same time at some point in space; in other words, $\phi(\omega)$ should be a linear function of ω. In such systems, a transform-limited seed pulse enters the system and the amplified pulse comes out still being transform limited. However, it is difficult to achieve ideal compression in reality. How does a nonideal compressor affect the pulse duration? To answer this, we need to scrutinize the spectral phase of an ultrashort pulse. Mathematically, the acquired spectral phase from the entire system can be expressed as a Taylor expansion:[26]

$$\phi(\omega) = \phi(\omega_o) + \phi'(\omega_o)(\omega - \omega_o) + \frac{1}{2}\phi''(\omega_o)(\omega - \omega_o)^2$$

$$+ \frac{1}{6}\phi'''(\omega_o)(\omega - \omega_o)^3 + \cdots, \qquad (1)$$

where ϕ', ϕ'', and ϕ''' are the derivatives of the phase with respect to frequency and are known as the group delay, group-delay dispersion (GDD), and third-order dispersion (TOD), respectively. Each derivative is the sum of the contributions from all the individual components including the stretcher, optical materials, and the compressor in the system. From Eq. (1), the group delay can be derived:

$$T(\omega) = \frac{\partial \phi(\omega)}{\partial \omega} = \phi'(\omega_o) + \phi''(\omega_o)(\omega - \omega_o)$$

$$+ \frac{1}{2}\phi'''(\omega_o)(\omega - \omega_o)^2 + \cdots. \qquad (2)$$

This expression shows that nonzero $\phi''(\omega_o)$ and $\phi'''(\omega_o)$ cause different time delays across the spectral components of the pulse and that the delay difference for the two ends of the bandwidth is larger when the spectral bandwidth (denoted by $\omega - \omega_o$) is broader. This is the reason why GDD and TOD play larger roles in a laser system using a broader spectrum. For extremely short pulses (<10 fs or so), even higher-order dispersion has to be considered in the system design.

In an ideal amplifier where a grating-pair stretcher and compressor are used, and there is no material dispersion, the system can be carefully designed and aligned in a manner that the sign for the spectral phase of the stretcher is opposite to the compressor for each order. Such an arrangement is called a matched stretcher and compressor. In reality, material dispersion has to be considered since it introduces GVD and higher-order dispersion. Therefore, the stretcher and/or compressor angle and separation has to be offset from the matched arrangement to compensate for the material dispersion. It is not difficult to just compensate for the GDD introduced by the material dispersion such that GDD=0 for the whole system. This is accomplished by manipulating the separation of either the stretcher grating pair or the compressor grating pair. However, it is difficult to simultaneously achieve GDD=0 and TOD=0 for the entire system. The GDD and TOD of a grating pair are coupled through the grating separation and angle such that when one offsets the grating separation to achieve total GDD=0, unwanted TOD might be introduced into the system, and vice versa. Experimentally, the grating separation and angle need to be adjusted iteratively to obtain the shortest pulse width from the system. Often, residual cubic spectral phase (TOD) exists even after the iteration procedure. This is one of the major problems that keeps one from obtaining <30 fs pulses from an amplifier system, not to mention the gain-narrowing effect in the amplifier medium.[26]

3. MODELING

We will model a THz system based on a CPA system and an EO polymer emitter–sensor pair. We first consider laser-related issues. Since it is always easier to compensate the linear chirp in a CPA system, it is reasonable that we assume that pulses from the CPA possess only second-order chirp, or cubic phase. We need to derive a mathematical expression of such a pulse. For this purpose, we first assume a transform-limited Gaussian pulse

with central frequency ω_o, half-width T_o of the pulse at $1/e$ of the intensity, and amplitude E_o, so its electric field can be written as

$$E_{in}(t) = E_o \exp(-t^2/2T_o^2)\exp(i\omega_o t). \qquad (3)$$

We can easily transform Eq. (3) to the frequency domain, which is

$$\tilde{E}_{in}(\omega) = E_o T_o \exp[-(\omega - \omega_o)^2 T_o^2/2]. \qquad (4)$$

Then, to express the pulse with cubic phase from the nonideal CPA, we modify Eq. (4) by adding the cubic spectral phase:

$$\tilde{E}_{in}(\omega) = E_o T_o \exp[-(\omega - \omega_o)^2 T_o^2/2]\exp[i\tau_3^3(\omega - \omega_o)^3], \qquad (5)$$

where τ_3^3 is the residual TOD, obtained from the CPA, with the unit of fs^3. We dropped the spectral terms ϕ and ϕ' because they give only a constant phase shift and a shift in time of the maximum of the pulse envelope, respectively, which does not affect the pulse width. When propagating in a dispersive medium, such a pulse acquires additional spectral phase terms contributed from the medium, and can be described as

$$\tilde{E}(z,\omega) = E_o T_o \exp[-(\omega - \omega_o)^2 T_o^2/2]\exp[i\tau_3^3(\omega - \omega_o)^3]$$

$$\times \exp\left[i\frac{zn_g}{c}(\omega - \omega_o) + i\frac{\beta_2 z}{2}(\omega - \omega_o)^2\right], \qquad (6)$$

where $n_g = n - \lambda_o(dn/d\lambda)_{\lambda_o}$ is the group index of the medium, z is the propagation distance, and $\beta_2 = d(1/\nu_g)/d\omega = d(n_g/c)/d\omega = (\lambda_o^3/2\pi c^2)(d^2 n/d\lambda^2)_{\lambda_o}$ is a parameter to describe the GVD of an optical medium. It should be noted that $\beta_2 z$ is the GDD defined in Section 2.

Now let us consider the THz generation site. The problem will become easier if it can be reduced to one dimension. The justification of a one-dimensional approximation requires that the emitter thickness be small with regard to the divergence of both the laser beam and the THz beam. Quantitatively, the Rayleigh length $\pi w_o^2/\lambda$ (w_o is the minimum beam waist of a Gaussian beam and λ is the wavelength) is used to determine the maximum distance that a Gaussian beam is collimated while propagating away from its minimum beam waist. For a laser beam, if we consider an extreme case where the beam waist of a focused 800 nm wavelength pump beam is only ∼100 μm, the corresponding Rayleigh length will be ∼39 mm. The emitter in our experiments is separated by less than 20 mm from the pump beam waist. Thus, as a first approximation, we can use the spot size of the pump beam at the emitter, which is close in size to the pump beam waist, as the beam waist of the generated THz beam. For the THz beam, if we consider the frequency component of 10 THz (30 μm in wavelength), which is at the higher end of our experimentally obtained spectra, the corresponding Rayleigh length is ∼1 mm, with lower frequency components having longer Rayleigh lengths. The emitter thickness in our experiments is usually much shorter than 1 mm, so it is justified that we take a thin-emitter assumption and solve a one-dimensional problem accordingly. Neglecting the pump beam depletion due to the conversion of optical pump power to THz power, the

OR effect,[27] which is actually a difference-frequency generation process, can be described by the following general one-dimensional nonlinear wave equation:[25]

$$\left[\frac{d^2}{dz^2} + \epsilon(\Omega)\frac{\Omega^2}{c^2}\right]\widetilde{E}_{THz}(z,\Omega) = \frac{4\pi}{c^2}\Omega^2 P_{NL}(z,\Omega), \qquad (7)$$

where c is the speed of light, Ω is the THz frequency, $\epsilon(\Omega)$ is the dielectric constant of the nonlinear medium (EO polymer, in our case) in the THz region, $\widetilde{E}_{THz}(z,\Omega)$ is the propagating THz field generated in the nonlinear medium, and $P_{NL}(z,\Omega)$ is the nonlinear polarization propagating along the z axis. $P_{NL}(z,\Omega)$ is the driving source for the generation of the THz wave and is related to the pump laser pulse and effective nonlinear susceptibility $\chi_{eff}(\Omega;\omega,\omega-\Omega)$ through the following equation:

$$P_{NL}(z,\Omega) = \int_{-\infty}^{\infty}\chi_{eff}(\Omega;\omega,\omega-\Omega)\widetilde{E}(z,\omega)\widetilde{E}^*(z,\omega-\Omega)d\omega. \qquad (8)$$

If the pump beam is far away from the material's electronic resonance region, $\chi_{eff}(\Omega;\omega,\omega-\Omega)=\chi_{eff}(\Omega)$ is independent of the pump beam wavelength, which is the situation in most THz generation systems. For this case, the nonlinear polarization can be simplified:

$$P_{NL}(z,\Omega) = \chi_{eff}(\Omega)\int_{-\infty}^{\infty}\widetilde{E}(z,\omega)\widetilde{E}^*(z,\omega-\Omega)d\omega. \qquad (9)$$

Using the expression for the pump beam field $\widetilde{E}(z,\omega)$ in Eq. (6) and evaluating the integral in Eq. (9), the nonlinear polarization is found to be

$$P_{NL}(\Omega) = \frac{\sqrt{\pi}T_o^2 E_o^2 \chi_{eff}(\Omega)}{\sqrt{T_o^2 - i3\tau_3^3\Omega}}$$
$$\times\exp\left(-\frac{T_o^2\Omega^2}{2}\right)\exp\left[\frac{(T_o^2\Omega + i\beta_2 z\Omega - i3\tau_3^3\Omega^2)^2}{4(T_o^2 - i3\tau_3^3\Omega)}\right]$$
$$\times\exp\left[i\left(\frac{n_g z}{c}\Omega - \frac{\beta_2 z}{2}\Omega^2 + \tau_3^3\Omega^3\right)\right]. \qquad (10)$$

For the case of our polymer THz emitters, $\chi_{eff}(\Omega)$ is approximately a constant in the THz range as they have no associated lattice structure. If the optical absorption coefficient α of the EO medium is also taken into consideration, the nonlinear polarization is then given by

$$P_{NL}(\Omega) = \frac{\sqrt{\pi}T_o^2 E_o^2 \chi_{eff}(\Omega)}{\sqrt{T_o^2 - i3\tau_3^3\Omega}}\exp\left(-\frac{T_o^2\Omega^2}{2}\right)$$
$$\times\exp\left[\frac{(T_o^2\Omega + i\beta_2 z\Omega - i3\tau_3^3\Omega^2)^2}{4(T_o^2 - i3\tau_3^3\Omega)}\right]$$
$$\times\exp\left[i\left(\frac{n_g z}{c}\Omega - \frac{\beta_2 z}{2}\Omega^2 + \tau_3^3\Omega^3\right)\right]\exp(-\alpha z). \qquad (11)$$

Obviously, from Eqs. (10) and (11), the nonlinear spectral phase of the pump pulses due to the nonideal compression of the CPA and the material dispersion of the EO medium contribute to the complexity of the spectral amplitude and phase for the nonlinear polarization. The existence of the residual TOD (τ_3^3, in our case) from the CPA reduces the spectral amplitude of the nonlinear polarization. For larger TOD and Ω, the reduction is more, which implies that the THz bandwidth is reduced. Similarly, the GVD parameter β_2 of a dispersive EO material also results in a reduction of the THz bandwidth. In addition, β_2 and TOD also appear in the spectral phase of P_{NL}, so they will also affect the phase-matching conditions for THz generation. This effect varies with the THz frequency and propagation distance in a complicated manner.

Because of the complexity of P_{NL}, there is no known analytical solution for Eq. (7). Therefore, we numerically solve Eq. (7) with boundary conditions $\widetilde{E}_{THz}(0,\Omega)=0$ and $d\widetilde{E}_{THz}(z,\Omega)/dz|_{z=0}=0$.[25] In our method we do not assume the slowly varying amplitude approximation that is frequently taken to find analytical solutions for many wave-mixing problems. It has been recognized, mostly through experiments, that phase-matching conditions (the difference between n_g and n_{THz})[28] and laser-pulse width dramatically affect the achievable THz emission bandwidth, but little simulation work has been applied to such issues. Recently, to investigate the role of phase mismatching on optical generation, van der Valk *et al.* conducted systematic studies by using ZnTe emitters of different thicknesses and varying the wavelength of the pump beam emitted from a $\sim$150 fs optical parametric oscillator.[29] Because the achieved bandwidth was only $\sim$2.5 THz in their case, the lattice resonance [$\sim$5.3 THz (Ref. 30)] and the corresponding dispersion and absorption of ZnTe in the THz regime was not a concern. This led to good agreement between their experiments and their simple model on the minima of the oscillating THz spectra. To our knowledge, no systematic study has been done to understand the effect of pump pulse distortion and EO material dispersion on THz emission. Yet complete simulation work on THz emission is desirable for researchers who want to predict the performance of a THz system so as to select suitable EO materials and light sources. With our numerical method, we can investigate the role each of these parameters plays. The fact that $\chi_{eff}(\Omega)$ is approximately constant and $\epsilon(\Omega)\approx n_{THz}^2(\Omega)$ is also approximately constant in amorphous EO polymers, due to the lack of a lattice resonance, makes such modeling work easy in comparison with crystalline EO materials. In the case of crystalline materials it is necessary to have an accurate model describing dispersion in the THz regime, which, unfortunately, is rarely available.

At the detection site, according to the model developed by Gallot and Grischkowsky, where the slowly varying approximation was taken, the response function of an EO sensor is given by[23]

$$f(d,\Omega) = C_{opt}(d,\Omega)\chi_{eff}(\omega;\Omega,\omega-\Omega)$$
$$\times\frac{\exp\left[i\frac{\Omega}{c}d(n_g - n_{THz})\right] - 1}{i\frac{\Omega}{c}(n_g - n_{THz})}, \qquad (12)$$

where d is the thickness of the sensor, and $C_{opt}(d,\Omega)$ $= \int_{-\infty}^{\infty} E(d,\omega)E^*(d,\omega-\Omega)d\omega$ is the autocorrelation of the electric field of the probe beam. In the original work of Gallot and Grischkowsky,[23] transform-limited pulses were assumed, which was valid when they used ~100 fs FWHM probe pulses. The effect of phase mismatching on the measurement bandwidth of the EO sampling was discussed in detail in that work, so we will not discuss this issue here. In our case, we employ the expression of the electric field in Eq. (6) with Eq. (12), and the response function $f(d,\Omega)$ is found to be

$$
\begin{aligned}
f(d,\Omega) = &\frac{\sqrt{\pi}T_o^2 E_o^2 \chi_{eff}(\omega;\Omega,\omega-\Omega)}{\sqrt{T_o^2 - i3\tau_3^3\Omega}} \\
&\times \exp\left(-\frac{T_o^2\Omega^2}{2}\right)\exp\left[\frac{(T_o^2\Omega + i\beta_2 d\Omega - i3\tau_3^3\Omega^2)^2}{4(T_o^2 - i3\tau_3^3\Omega)}\right] \\
&\times \exp\left[i\left(\frac{n_g d}{c}\Omega - \frac{\beta_2 d}{2}\Omega^2 + \tau_3^3\Omega^3\right)\right] \\
&\times \frac{\exp\left[i\frac{\Omega}{c}d(n_g - n_{THz}) - 1\right]}{i\frac{\Omega}{c}(n_g - n_{THz})}.
\end{aligned}
\tag{13}
$$

According to Kleinman's symmetry,[31] $\chi_{eff}(\omega;\Omega,\omega-\Omega)$ $= \chi_{eff}(\Omega;\omega,\omega-\Omega)$. In our specific case of EO polymers, they are the same constant. Except for the last term representing the phase-matching factor, the expression of $f(d,\Omega)$ is exactly the same as that of P_{NL} [see Eq. (10)], with the sensor thickness d replacing the emitter thickness z. This can be explained by the use of a nonresonant EO and OR effect where C_{opt} and P_{NL} have the same form [neglecting the constant $\chi_{eff}(\Omega)$ term contained in P_{NL}]. The THz spectrum obtained from the system is then $S_{THz}(z,d,\Omega)$ $= E_{THz}(z,\Omega)f(d,\Omega)$, where we have, for simplicity, ignored propagation effects such as diffraction and overlapping between the THz beam and probe beam at the sensor position (related to the alignment in real experiments). The material absorption in the optical regime can be easily added to $f(d,\Omega)$, just as in the case of P_{NL}. To focus on the most important factors that affect the performance of a THz system, we will not consider the optical absorption of an emitter and sensor material in this section. However, this effect, which itself is not frequency dependent, decreases the entire THz signal, leading to a lower bandwidth above the noise level. Thus, in Section 4 we take the optical absorption of the EO polymer films into consideration so as to make the experimental and simulation results agree.

To study the effects of laser pulses on the THz bandwidth, we do simulations of two cases where transform-limited and non-transform-limited pulses are involved. For the first case, we assume two transform-limited Gaussian pulses with the same pulse energy and spectral bandwidths of 90 and 9 nm FWHM. For a transform-limited Gaussian pulse, its time–bandwidth product follows $\Delta t_{FWHM}\Delta\nu_{FWHM} = 0.441$, where $\Delta\nu_{FWHM}$ $= (c/\lambda^2)\Delta\lambda_{FWHM}$. Once the spectral bandwidth is known, the pulse width is known too. [It should be noted that

Δt_{FWHM} is related to T_o—the half-width at $1/e$ of the amplitude of the laser intensity by $\Delta t_{FWHM} = 2(\ln 2)^{1/2}T_o$.] In our specific cases of 90 and 9 nm spectral bandwidths in FWHM, the corresponding pulse durations in FWHM are 10 and 100 fs, respectively. Figure 1 shows the THz amplitude spectra that are obtained from these two pulses (solid curves) using an 80 μm thick emitter and a 100 μm thick sensor made of an EO polymer that has been assigned an optical group index $n_g = 1.93$ and a THz group index $n_{THz} \approx 1.73$ (we will see in Section 4 that these values correspond to the EO polymer LAPC). As shown in Fig. 1, the broader spectral bandwidth of the 10 fs FWHM laser pulse results in a broader observable THz bandwidth (black solid curve) in comparison with the bandwidth corresponding to the 100 fs FWHM laser pulse (gray solid curve) if the same minimum detection level is assumed. Because of the presence of phase mismatching (discussed below), the spectral dip around 15 THz is due to the thickness of the LAPC sensor and the spectral dip around 18.5 THz is due to the thickness of LAPC emitter. In the case of the 9 nm FWHM transform-limited pulse, no spectral dip can be seen above the assumed minimum detection level.

For the second case, we consider the influence of the cubic phase distortion of the pulses. The nature of the wave-mixing processes for the OR effect makes it obvious that a broader laser spectral bandwidth translates into a broader THz wave bandwidth, which has already been demonstrated by the simulation shown in Fig. 1. On the other hand, we also know that a broader spectral bandwidth does not guarantee a shorter pulse width if the spectral phase distortion (GDD, TOD, and higher-order dispersion) is not well taken care of. As shown in the expression of the nonlinear polarization P_{NL} [see Eq. (10)], the presence of τ_3^3 in a pump pulse should result in a reduction of the THz spectrum. To show this effect by simu-
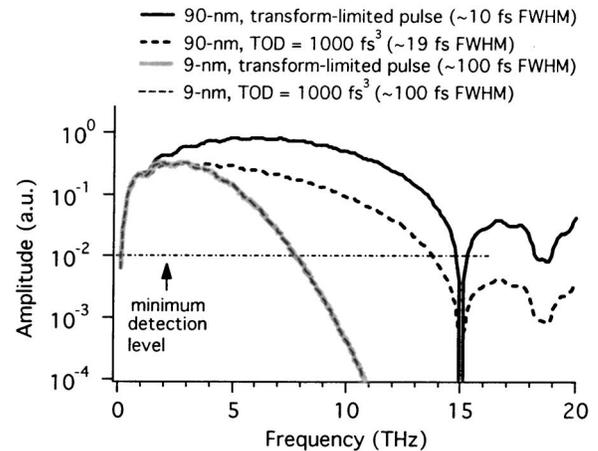

Fig. 1. Simulated THz amplitude spectra corresponding to a transform-limited pump pulse with 90 nm FWHM spectral bandwidth (black solid curve), a non-transform-limited pulse with 90 nm FWHM spectral bandwidth and 1000 fs³ TOD (thick dashed curve), a transform-limited pulse with 9 nm FWHM spectral bandwidth (gray solid curve), and a non-transform-limited pulse with 9 nm FWHM spectral bandwidth, and 1000 fs³ TOD (thin dashed curve). In all the cases, an 80 μm thick EO polymer emitter and a 100 μm thick EO polymer sensor are assumed. For comparison, the same hypothetical minimum detection level (determined by the detection scheme of the system) is also assumed.

lation, we assume $\tau_3^3 = 1000$ fs^3 for the two Gaussian pulses. The simulated THz amplitude spectra are shown as the dashed curves in Fig. 1. The TOD plays an important role for the pulse with a 90 nm FWHM spectral bandwidth: We observe a lower amplitude and narrower bandwidth (thick dashed curve) compared with the spectrum corresponding to the transform-limited pulse with the same spectral bandwidth (black solid curve). Intuitively, the TOD-induced pulse widening in the pulse with a broad spectrum causes a decrease in the pump intensity, leading to a decrease of the THz signal amplitude. On the other hand, the TOD has no apparent effect on the pulse with only a 9 nm FWHM spectral bandwidth: The two THz spectra overlap well when TOD is and is not present in the pulses. Considering the quadratic relationship between the TOD-induced pulse widening and the bandwidth [see Eq. (2)], with TOD = 1000 fs^3, the duration of the pulse with the 90 nm FWHM spectral bandwidth is estimated to be broadened by ~9 fs (using $\Delta T \sim \text{TOD}(\Delta\omega/2)^2/2$, where $\Delta\omega$ is the spectral bandwidth expressed in radians); whereas the pulse with the 9 nm FWHM spectral bandwidth widens slightly, which explains qualitatively why THz generation is not affected by the existence of TOD in this case. In these simulations, the EO polymer is assumed to have no optical dispersion ($\beta_2 = 0$).

OR is an interaction between a light pulse and an EO medium. So far, we have discussed the influence of the pump laser pulses. How do the properties of an EO medium affect THz generation? This is an important question as the answer will provide us with a guide to material selection. For this purpose, we first consider phase mismatching[28] (the phase velocity of the THz wave differs from the group velocity of the pump pulse when $n_g \neq n_{\text{THz}}$), which is a highly important factor that affects the THz emission. All of the inorganic EO crystals that are commonly used for THz generation and detection possess lattice resonances in the THz range. For example, ZnTe has a transverse-optical (TO) phonon resonance around 5.3 THz,[30] GaAs has a TO phonon resonance around 8.0 THz,[30] and the inability of all the existing broadband THz systems based on GaSe to exhibit a signal below ~7 THz might be due to the existence of single or multiple lattice resonances in this range that have not yet been characterized. Because of these lattice resonances, the THz indices $n_{\text{THz}}(\Omega)$ change significantly in the THz emission–detection range in any crystalline EO medium. As a result, there is not a single optical wavelength at which the material has the optical group index perfectly matched with the whole range of THz frequencies. For example, at 800 nm, ZnTe has good phase matching only for a narrow range around ~2 THz.[28] A lattice resonance also results in a fast varying $\chi_{\text{eff}}(\Omega)$ in the region around it. On the other hand, amorphous EO polymer materials are expected to have approximately constant $n_{\text{THz}}(\Omega)$ and $\chi_{\text{eff}}(\Omega)$ in the whole THz emission–detection frequency range because of the lack of a lattice structure. Our n_{THz} measurement of LAPC based on THz TDS demonstrates this, as shown in Fig. 2. The thickness of LAPC under investigation was ~400 μm. This can be considered to be optically thick because the travel time of each round trip for Fresnel reflection inside the sample, or the separation
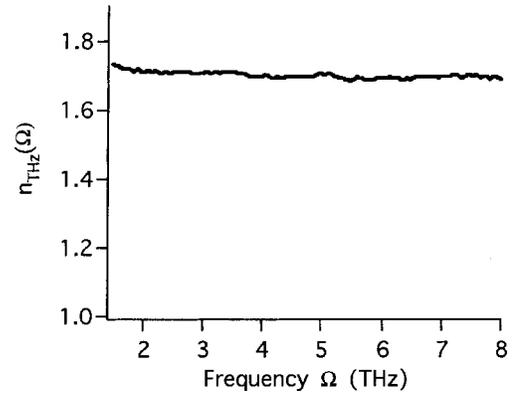

Fig. 2. THz index $n_{\text{THz}}(\Omega)$ of LAPC, measured using THz TDS. For a wide range between ~1.5 and ~8 THz, $n_{\text{THz}}(\Omega)$ is approximately constant. Because of the low dynamic range for the frequency components below ~1.5 THz in our THz TDS experiments based on a LAPC emitter and sensor pair, the extracted THz indices in that range are not reliable and are not shown in the figure.

between the THz transient echoes, was ~4.5 ps (determined by $2tn_g/c$, where t is the sample thickness and n_g is the group index of the THz wave, which is close to n_{THz} in our specific case of EO polymers) while we only commanded our optical delay line to travel a limited distance such that the first THz transient echo did not appear. To prepare such a thick sample, we used a casting method followed by a film pressing process. The achieved surface flatness is ~5%, so the thickness of the whole area of the sample was 400 ± 20 μm. The uncertainty of the sample thickness affects the accuracy of the extracted n_{THz} through the following relation:[32]

$$\Delta n \approx \frac{\Delta x}{t} + |n_{\text{THz}} - 1|\frac{\Delta t}{t}, \qquad (14)$$

where Δx is the resolution of the delay line (1 μm in the experiments), and Δt is the uncertainty of the sample thickness. In our case, the first term is much smaller than the second term and can be neglected. Because of the presence of Δt, Δn has a magnitude of ~0.04.

The feature of a constant n_{THz} makes it quite easy to see the effect of phase mismatching by using different values of n_{THz} in the simulations. If we imagine two different EO polymers, 1 and 2 (both have the same EO coefficient), EO polymer 1 is the material ($n_g = 1.93$, $n_{\text{THz}} = 1.73$) used for the above simulations, while EO polymer 2 is assigned with the same n_g as EO polymer 1, but with $n_{\text{THz}} = 1.91$. In Fig. 3 our simulation results show that the emitter–sensor pair made out of EO polymer 2 (thick dashed curve) provides a much broader and flatter THz spectrum than a pair made out of EO polymer 1 (thin dashed curve). For the above simulations, we have assumed 80 μm for the emitter thickness, 100 μm for the sensor thickness, and a transform-limited 10 fs FWHM Gaussian pulse with TOD = 0. It is expected that when perfect phase matching can be achieved, the THz bandwidth will be limited only by the spectral bandwidth of the pump pulses and the minimum detection level of the system.

In addition to a broader achievable bandwidth, from Fig. 3 we also see that the good phase matching leads to a brighter emission (the area under the amplitude spec-

trum). What is more, with good phase matching it is possible to get even brighter THz emission by increasing the thickness of the emitters. Figure 3 shows the changes of THz emission brightness when the thickness of emitters is changed for both EO polymers. For the emitters made of EO polymer 1, increasing the thickness from 80 (thin dashed curve in Fig. 3) to 600 μm (thin solid curve in Fig. 3) does not provide an obviously brighter THz emission, and even worse, it causes several spectral dips due to the existing phase-mismatching situation; in contrast, for EO polymer 2, increasing the thickness from 80 (thick dashed curve in Fig. 3) to 600 μm (thick solid curve in Fig. 3) does lead to a brighter THz emission. If we can find a perfect phase-matching material and this material possesses β_2 =0, the THz amplitude should linearly increase with the emitter thickness. As an alternative to the approach of accessing bright THz sources by seeking EO materials with extremely high EO coefficients, we can use thick emitters made out of EO polymers with reasonable EO coefficients and good phase-matching properties. For this purpose, polymer engineering has shown potential that cannot be expected from inorganic materials. Many EO polymers with impressively high EO coefficients have become available, driven by the telecommunication industry's desire for inexpensive EO device integration. With the well-developed THz TDS technique we can select from the available EO polymers those possessing good phase-matching properties (for suitable light sources) and make long waveguiding THz emitters. This is one of the noticeable advantages for using EO polymers as THz emitters.

We now consider another important yet frequently neglected material-related issue—GVD. According to Sec-
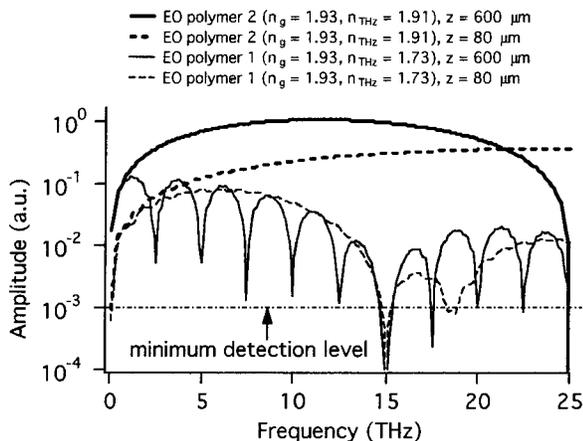

Fig. 3.   Comparison of simulated THz amplitude spectra for emitters made of EO polymers with different phase-matching conditions and thicknesses when we used a laser pulse of 10 fs FWHM in duration and a 100 μm thick sensor made of the same material as the emitter. Because of the better phase-matching property of EO polymer 2, the 80 μm thick emitter (thick dashed curve) shows a broader bandwidth and brighter emission (the area under the spectrum) than the emitter made of EO polymer 1 (thin dashed curve). When the thickness of the THz emitter made of the EO polymer 2 is increased from 80 (thick dashed curve) to 600 μm, (thick solid curve), there is an apparent brighter THz emission, denoted by the increase of the area under the amplitude spectrum. However, for the emitter made of EO polymer 1, when the thickness is increased from 80 (thin dashed curve), to 600 μm (thin solid curve), the THz emission brightness is not increased, but spectral dips, due to the phase mismatching, also appear.

tion 2, GVD effects broaden a shorter pulse more seriously than a wider pulse because the former is associated with a broader spectral bandwidth. As many ultrabroadband optical THz systems have routinely employed pulse with a duration <15 fs FWHM, it is important to study how the pulse distortion due to GVD in an EO medium affects the performance of such systems. In parallel with the phase-matching study we just presented, this study can provide us an additional guide to select suitable materials and light sources. As we did in the study of pulse distortion on the performance of an optical THz system, we do simulations for two cases where 10 and 100 fs FWHM transform-limited pulses are used. In both cases, we use EO polymer 2 because it has good phase-matching properties and studying the GVD effects in this material can clearly show the importance of this additional consideration for material selection. We assume that EO polymer 2 has β_2=1.859 fs^2/μm, which is the actual value for our EO polymer LAPC at an optical wavelength of 800 nm. Assuming τ_3^3=0 fs^3 for the nonlinear polarization $P_{NL}(z,\Omega)$ [see Eq. (10)] and the response function $f(d,\Omega)$ [see Eq. (13)], we can immediately see that the inclusion of β_2 causes reduced THz emission strength–detection sensitivity and bandwidth. The reduction is worse when a broader THz bandwidth (higher Ω) resulting from a broader laser spectral bandwidth is involved. Our simulation results using 10 fs FWHM pulses, shown in Fig. 4(a), demonstrate this. The THz bandwidth corresponding to the 80 μm emitter made of EO polymer 2 with β_2 taken into consideration (thin dashed curve) is significantly narrower than the THz bandwidth corresponding to the same emitter with β_2 neglected, (thin solid curve); when the emitter thickness is increased to 400 μm, the bandwidth with β_2 considered (thick dashed curve) is still much narrower than that with β_2 neglected (thin solid curve). It is also interesting to observe from Fig. 4(a) that, even for the 80 μm emitter, the reduction of bandwidth and brightness is significant with the consideration of β_2, and that an increase of emitter thickness from 80 to 400 μm only slightly changes the THz spectral amplitude, in contrast to the case where β_2 is neglected. On the other hand, when 100 fs FWHM pulses are used, the GVD effect does not play an observable role, as shown in Fig. 4(b). For the simulations above, a 100 μm thick sensor is assumed. In addition to the frequency-domain explanation, we can also understand the influence of GVD effects in the time domain by investigating the pulse widening in a dispersive medium using the following equation:[33]

$$\tau_{out} = \tau_{in} \left[1 + 16 \frac{(\beta_2 z)^2}{\tau_{in}^2} (\ln 2)^2 \right]^{1/2}, \qquad (15)$$

where τ_{in} is the incident pulse (transform-limited) duration in FWHM, and τ_{out} is the exiting pulse duration in FWHM from a dispersive medium. In the case where a 10 fs FWHM transform-limited pulse passes through EO polymer 2, the pulse duration becomes 42 and 206 fs in FWHM at an 80 and 400 μm distance, respectively; for a 100 fs FWHM transform-limited incident pulse in the same material and at the same distances, the pulse durations are 100 and 102 fs in FWHM (very slight change). According to this simple calculation, clearly, in the same
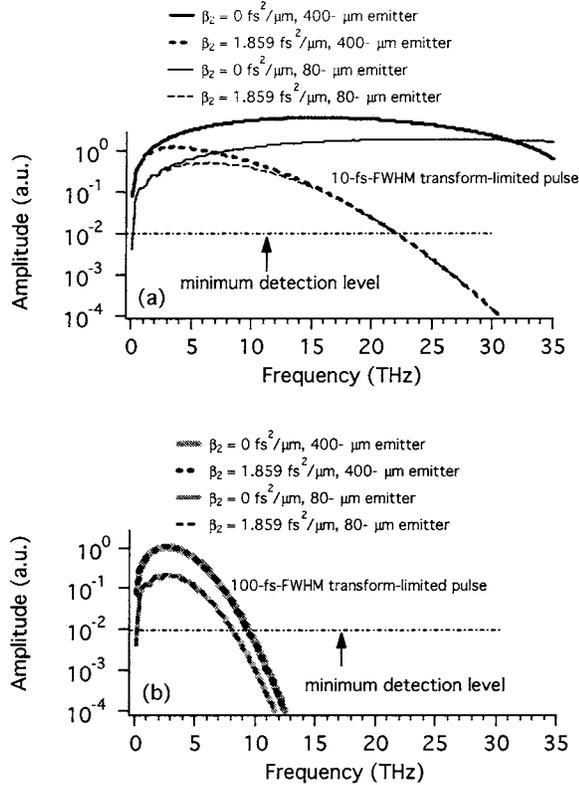
Fig. 4. GVD effect on the performance of the emitter–sensor pairs made of EO polymer 2 when (a) 10 fs FWHM transform-limited pulse is used and (b) 100 fs FWHM transform-limited pulse is used. In (a), the inclusion of GVD, or β_2, causes significant reduction of the THz spectral bandwidth and brightness for both 80 μm (thin solid curve for $\beta_2=0$, thin dashed curve for $\beta_2=1.859$ fs$^3/\mu$m) and 400 μm (thick solid curve for $\beta_2=0$, thick dashed curve for $\beta_2=1.859$ fs$^3/\mu$m) emitters. In (b), GVD does not play an observable role for both 80 μm (gray thin solid curve for $\beta_2=0$, black thin dashed curve for $\beta_2=1.859$ fs$^3/\mu$m) and 400 μm (gray thick solid curve for $\beta_2=0$, black thick dashed curve for $\beta_2=1.859$ fs$^3/\mu$m) emitters.

dispersive medium a very short pulse is broadened much more than its wider counterpart. Using Eq. (2), we can also estimate the pulse broadening ($\Delta T \sim$ GDD$\Delta\omega$, where GDD$=\beta_2 z$). The results from the two methods are not exactly the same, with Eq. (15) being more accurate, but the discrepancy is less than 20%. The pulse broadening eliminates part of the achievable THz bandwidth and brightness that is potentially offered by an extremely short pulse. Therefore, low dispersion is another requirement for an EO medium used as a THz emitter–sensor pair in addition to good phase-matching properties to achieve high-brightness and broad-bandwidth THz emission.

4. COMPARISON OF THE SIMULATIONS WITH EXPERIMENTS

To test our model, we need to investigate the agreement between our simulation and experimental results. In our experiments, we used a CPA emitting a 1 kHz, ~45 fs FWHM pulse train with a spectral bandwidth of ~23 nm centered at 800 nm and LAPC emitter–sensor pairs. By fitting the data of the refractive index measurement on LAPC to a Sellmeier dispersion formula, the dispersion of

LAPC (its birefringence is so weak that it can be neglected) can be expressed as $n^2=2.3045+(0.33636 \times \lambda_{opt}^2)/(\lambda_{opt}^2-0.512^2)$,[15] where λ_{opt} is the optical wavelength in micrometers. The peak absorption wavelength for LAPC is 0.512 μm. Using the formula, the optical refractive index n of LAPC at 800 nm is calculated to be 1.70, the optical group index $n_g \approx 1.93$, and the group-velocity parameter $\beta_2=1.859$ fs$^2/\mu$m. The THz index of LAPC $n_{THz} \approx 1.70 \pm 0.04$ was obtained by THz TDS (described above). To have LAPC emitters with different thicknesses, we prepared four layers of freestanding LAPC films using a 75 μm thick spacer to control their thicknesses. The obtained films were ~75 μm thick with an inaccuracy of ±10%. We then stacked them up for various emitter thicknesses. We also prepared a LAPC film using a 120 μm thick spacer for the THz sensor, leading to the real film thickness of 120±12 μm. Considering the poling geometry and the p polarization of the pump beam in the experiments,[15] we oriented the polymer emitter away from the normal incidence by ~59°, the Brewster angle corresponding to the optical refractive index of LAPC (1.70 at 800 nm), for the highest THz emission. With this incidence angle, the refraction angle inside the polymer is ~30°. The effective thickness of each film used as an emitter is 75/cos(30°)≈87.0 μm plus the thickness uncertainty of ±10%. It should also be noted that a small incidence angle deviation from 59° in the experiments also contributes to an error of the effective thickness estimation. For example, if the real incidence angle is ~55°, the effective thickness should be ~85.7 μm instead of ~87.0 μm. Similarly, with the orientation for the sensor (~45°), we estimate our sensor with an effective thickness of 132 μm plus the uncertainty of ±10%. Experimentally obtained spectra are shown as dashed curves in Fig. 5 for one-, two-, three-, and four-layer emitters. In the case of three- and four-layer LAPC emitters, spectral dips are observed. We then did simulations to fit these experimental spectra. With perfect pulse compression, a 23 nm spectral bandwidth can support a transform-limited ~41 fs FWHM pulse. In our experiment, we had ~23 nm spectral bandwidth and ~45 fs FWHM pulse duration, which implies that the pulses were not transform limited.

Using our Grenouille, a pulse characterization instrument employing the scheme of frequency-resolved optical gating,[34] we identified evidence of cubic phase distortion for the pulses out of the CPA. Considering the measured pulse width and spectral bandwidth, we estimated TOD ~5000 fs^3 for the laser pulses in our experiments and took this into consideration in our simulations. To fit our simulations to the experimental results, we found that $n_{THz}=1.73$ delivers the best results (this value of n_{THz} is still within a reasonable error range for LAPC). We also found it necessary to slightly vary the effective thickness of our emitters and sensor in reasonable ranges (due to the uncertainty of the film thicknesses and incidence angle) to best fit the experiments.

The simulated THz spectra are shown as solid curves in Fig. 5 to be compared with their corresponding experimental results. For the best fitting, the 85, 165, 255, and 350 μm emitters and 120 μm sensor thicknesses were used. The optical absorption coefficient of LAPC at 800 nm was measured to be 22.7 cm^{-1}, and this value was
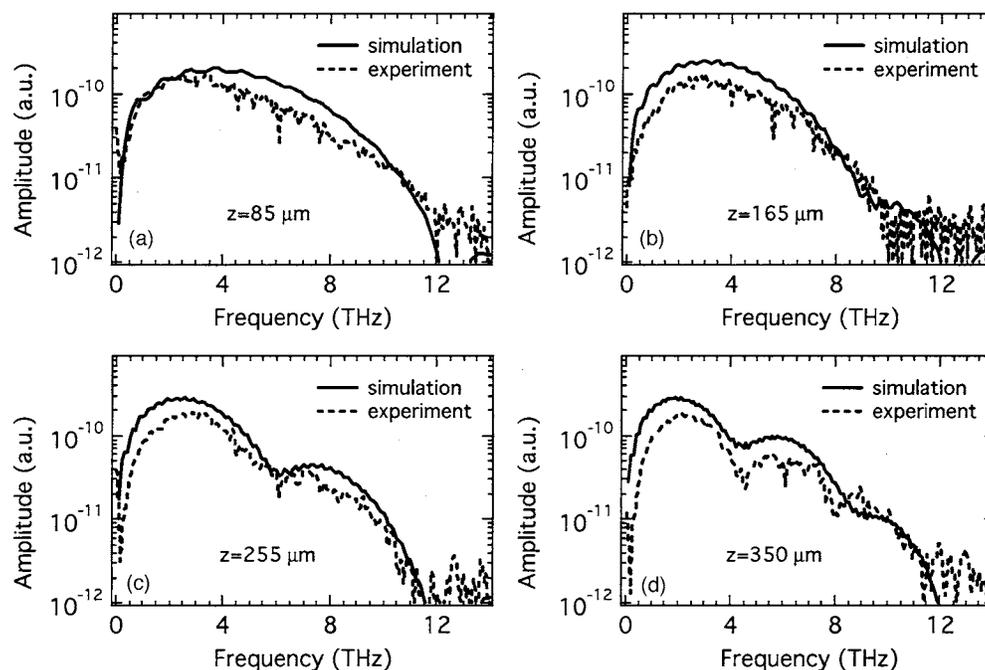
Fig. 5. Comparison of the simulation (solid curves) with experimental results (dashed curves) when a 120 μm (effective thickness) LAPC sensor and (a) 85 μm, (b) 165 μm, (c) 255 μm, and (d) 350 μm (effective thickness) LAPC emitters are used. TOD=5000 fs^3 is determined from the pulse width and spectrum measurements using our Grenouille and spectrometer. The error of the effective thicknesses of the emitters and the sensor is less than 10%. $n_{\mathrm{THz}}=1.73$ is selected such that the frequency locations of the phase-mismatching-induced spectral dips and the overall THz bandwidths have the best agreement between the simulations and experiments.

used in our simulation. Using these parameters, we can achieve good agreement between the simulations and experiments: All of the spectral dips in the experimental results are also present at the same frequency locations in the simulation results. For simplicity, we did not consider diffraction effects, and we also ignored water absorption (in our experiments, the air is not completely dry). The former assumption can explain the discrepancy in the low-frequency range and the latter can explain the higher-frequency discrepancies. In the cases of two-, three- and four-layer emitters, the discrepancies are relatively large in the low-frequency range. This is possibly due to the method by which the multiple samples were stacked—they were simply held in one corner by a plastic clamp. Because of this, they were not perfectly parallel nor completely contacting each other. Generally speaking, our model can quite successfully predict the performance, such as the overall bandwidth, frequency roll-off, and phase-mismatching-induced spectral dips, of a THz system based on an EO polymer emitter–sensor pair, since it is relatively easy to measure EO polymer properties in the optical and THz region. If accurate models for the dielectric response and nonlinearity of EO crystals can be obtained in the THz region, our model will work equally well for the materials.

5. CONCLUSIONS

We have developed a model to predict the performance of a THz system, including the brightness and bandwidth, using the OR effect of an EO medium for THz generation and EO sampling for THz detection. Most of the discus-

sion has been focused on THz generation. On the basis of an LAPC emitter–sensor pair, we have investigated the effects of both nonideal laser pulses and dispersive materials in an EO medium. Our model shows that transform-limited ultrashort pulses with broad spectral bandwidth and an EO medium with good phase matching for the optical pulses and the THz pulses, as well as low material dispersion, are essential to achieve bright and broadband THz emission. The simulation work based on this model fits well with our experimental results, demonstrating the validity of this model. The model can be used as a guide to select suitable EO polymers for THz generation and detection and may be helpful for the simulation of inorganic crystalline EO emitters as well, provided that an accurate description of the dielectric function $\epsilon(\Omega)$ and $\chi^{(2)}(\Omega)$ can be found for the material. Further improvement for this model should include the diffraction effect of the optics in the THz propagation path, as low-THz-frequency components, or longer wavelengths, can be lost due to this effect.

REFERENCES

1. R. A. Cheville and D. Grischkowsky, "Far infrared, THz time-domain spectroscopy of flames," Opt. Lett. **20**, 1646–1648 (1995).

2. D. Mittleman, R. H. Jacobsen, and M. Nuss, "T-ray imaging," IEEE J. Sel. Top. Quantum Electron. **2**, 679–692 (1996).

3. G. Gallot, J. Zhang, R. W. McGowan, T.-I. Jeon, and D. Grischkowsky, "Measurements of the THz absorption and dispersion of ZnTe and their relevance to the electro-optic detection of THz radiation," Appl. Phys. Lett. **74**, 3450–3452 (1999).

4. Y. C. Shen, P. C. Upadhya, E. Lindahl, and A. G. Davies, "Observation of far-infrared emission from excited cytosine molecules," Appl. Phys. Lett. **87**, 011105 (2005).

5. S. W. Smye, J. M. Chamberlain, A. J. Fitzgerald, and E. Berry, "The interaction between terahertz radiation and biological tissue," Phys. Med. Biol. **46**, R101–R112 (2001).

6. A. Rice, Y. Jin, X. F. Ma, X.-C. Zhang, D. Bliss, J. Larkin, and M. Alexander, "Terahertz optical rectification from ⟨110⟩ zinc-blende crystals," Appl. Phys. Lett. **64**, 1324–1326 (1994).

7. Q. Wu and X.-C. Zhang, "Free-space electro-optic sampling of terahertz beams," Appl. Phys. Lett. **67**, 3523–3525 (1995).

8. C. Fattinger and D. Grischkowsky, "Terahertz beams," Appl. Phys. Lett. **54**, 490–492 (1989).

9. C. Kubler, R. Huber, S. Tubel, and A. Leitenstorfer, "Ultrabroadband detection of multiterahertz field transients with GaSe electro-optic sensors: approaching the near infrared," Appl. Phys. Lett. **85**, 3360–3362 (2004).

10. A. Nahata, D. Auston, C. Wu, and J. T. Yardley, "Generation of terahertz radiation from a poled polymer," Appl. Phys. Lett. **67**, 1358–1360 (1995).

11. A. M. Sinyukov and L. M. Hayden, "Generation and detection of terahertz radiation with multilayered electro-optic polymer films," Opt. Lett. **27**, 55–57 (2002).

12. A. M. Sinyukov and L. M. Hayden, "Efficient electro-optic polymers for THz systems," J. Phys. Chem. B **108**, 8515–8522 (2004).

13. A. M. Sinyukov, M. R. Leahy, L. M. Hayden, M. Haller, J. Luo, A. K. Y. Jen, and L. R. Dalton, "Resonance enhanced THz generation in electro-optic polymers near the absorption maximum," Appl. Phys. Lett. **85**, 5827–5829 (2004).

14. H. Cao, T. F. Heinz, and A. Nahata, "Electro-optic detection of femtosecond electromagnetic pulses by use of poled polymers," Opt. Lett. **27**, 775–777 (2002).

15. X. Zheng, A. M. Sinyukov, and L. M. Hayden, "Broadband and gap-free response of a terahertz system based on a poled polymer emitter-sensor pair," Appl. Phys. Lett. **87**, 081115 (2005).

16. S. H. Han and J. W. Wu, "Single-beam polarization interferometry measurement of the linear electro-optic effect in poled polymer films with a reflection configuration," J. Opt. Soc. Am. B **14**, 1131–1137 (1997).

17. P. C. M. Planken, H.-K. Nienhuys, H. J. Bakker, and T. Wenckebach, "Measurement and calculation of the orientation dependence of terahertz pulse detection in ZnTe," J. Opt. Soc. Am. B **18**, 313–317 (2001).

18. Y. Shi, C. Zhang, H. Zhang, J. H. Bechtel, L. R. Dalton, B. H. Robinson, and W. H. Steier, "Low (sub-1-volt) half wave voltage polymeric electro-optic modulators achieved by controlling chromophore shape," Science **288**, 119–122 (2000).

19. J. Luo, M. Haller, H. Ma, S. Liu, T.-D. Kim, Y. Tian, B. Chen, S.-H. Jang, L. R. Dalton, and A. K.-Y. Jen, "Nanoscale architectural control and macromolecular engineering of nonlinear optical dendrimers and polymers for electro-optics," J. Phys. Chem. B **108**, 8523–8530 (2004).

20. A. Jen, J. Luo, T. Kim, B. Chen, S. Hau, L. Dalton, J.-W. Kang, D. Park, and W. Herman, "Exceptional electro-optic properties through supermolecular self-assembly," in *Frontier in Optics 2005/Laser Science XXI* (Optical Society of America, 2005), paper STuD1.

21. D. H. Park, C. H. Lee, W. N. Herman, J. W. Kang, J. D. Luo, T. D. Kim, and A. K.-Y. Jen, "Nonlinear ellipsometric analysis of the electro-optic effect in poled organic glasses," in *Frontier in Optics 2005/Laser Science XXI* (Optical Society of America, 2005), paper STuD4.

22. Q. Wu and X.-C. Zhang, "Design and characterization of traveling wave electro-optic terahertz sensors," IEEE J. Sel. Top. Quantum Electron. **2**, 693–700 (1996).

23. G. Gallot and D. Grischkowsky, "Electro-optic detection of terahertz radiation," J. Opt. Soc. Am. B **16**, 1204–1212 (1999).

24. L. Xu, X.-C. Zhang, and D. H. Auston, "Terahertz beam generation by femtosecond optical pulses in electro-optic materials," Appl. Phys. Lett. **61**, 1784–1786 (1992).

25. J. Faure, J. van Tilborg, R. A. Kaindl, and W. P. Leemans, "Modelling laser-based table-top THz sources: optical rectification, propagation and electro-optic sampling," Opt. Quantum Electron. **36**, 681–697 (2004).

26. S. Backus, C. G. Durfee, III, M. Murnane, and H. Kapteyn, "High power ultrafast lasers," Rev. Sci. Instrum. **69**, 1207–1223 (1998).

27. D. H. Auston and M. C. Nuss, "Electro-optical generation and detection of femtosecond electrical transients," IEEE J. Quantum Electron. **24**, 184–197 (1988).

28. A. Nahata, A. Weling, and T. F. Heinz, "A wideband coherent terahertz spectroscopy system using optical rectification and electro-optic sampling," Appl. Phys. Lett. **69**, 2321–2323 (1996).

29. N. C. J. van der Valk, P. C. M. Planken, A. N. Buijserd, and H. J. Bakker, "Influence of pump wavelength and crystal length on the phase matching of optical rectification," J. Opt. Soc. Am. B **22**, 1714–1718 (2005).

30. Q. Wu, M. Litz, and X. C. Zhang, "Broadband detection capability of ZnTe electro-optic field detectors," Appl. Phys. Lett. **68**, 2924–2926 (1996).

31. R. W. Boyd, *Nonlinear Optics*, 2nd ed. (Academic, 2003), pp. 36–37.

32. L. Duvillaret, F. Garet, and J.-L. Coutaz, "Highly precise determination of optical constants and sample thickness in terahertz time-domain spectroscopy," Appl. Opt. **38**, 409–415 (1999).

33. F. Salin and A. Brun, "Dispersion compensation for femtosecond pulses using high-index prisms," J. Appl. Phys. **61**, 4736–4739 (1987).

34. K. W. Delong, R. Trebino, J. Hunter, and W. E. White, "Frequency-resolved optical gating with the use of second-harmonic generation," J. Opt. Soc. Am. B **11**, 2206–2215 (1994).